

P-I diagrams for linear-elastic cantilevered Timoshenko beams including higher modes of vibration

L. J. van der Meer, J. G. M. Kerstens and M. C. M. Bakker

Faculty of Architecture, Building and Planning, Eindhoven University of Technology, Eindhoven, the Netherlands

Pressure-impulse (P-I) diagrams are commonly used to assess damage of structural components subjected to blast loading. The response to blast loading is characterized by three main aspects: (a) the excitation of higher modes of vibration, (b) strain rate effects, and (c) ductility. P-I diagrams are often based on equivalent single degree of freedom (SDOF) systems. These SDOF systems can take strain rate effects and ductility into account, to a certain extent, but the influence of higher modes is neglected. All three aspects can be incorporated in finite element simulations, but at the cost of generality and comprehensibility. For a better understanding, this theoretical study derives P-I diagrams including higher modes, without strain rate effects and ductility. These P-I diagrams are derived for a continuous, linear-elastic, cantilevered Timoshenko beam, which represents the load-bearing structure of a multistory building, subjected to idealized blast loading. The response is determined analytically using mode superposition. Modal contribution factors for dynamic base shear are derived, based on earthquake engineering. For the material behaviour and boundary conditions investigated, it is concluded that P-I diagrams based on equivalent SDOF systems are not conservative for short-duration (impulsive) loading, and non-uniform spatial load distributions. Moreover, the shape of the P-I diagrams that have been derived, deviates significantly from the hyperbolic shape of P-I diagrams for SDOF systems.

Key words: Pressure-Impulse diagram, Timoshenko beam, modal contribution factor, dynamic load factor, blast load, higher modes

1 Introduction

Pressure-impulse (P-I) diagrams or iso-damage curves are used to estimate resistance of structural components to blast or impact loading in the early design stage. The concept of P-I diagrams first appeared in the 1950s. Historical aspects of P-I diagrams are described in

Abrahamson and Lindberg [1976]. P-I diagrams are applicable to any type of non-periodic dynamic load with a finite duration. The structure or structural component to which this load is applied should have an unambiguous damage criterion. However, it is possible to combine P-I diagrams for different failure modes (e.g. shear and bending failure), as shown in Ma et al. [2007]. Text books featuring P-I diagrams (such as Smith and Hetherington [1994] and Kappos [2002]) are often based on equivalent single degree of freedom (SDOF) systems. P-I diagrams based on SDOF systems are directly linked to the dynamic load factor (DLF). Both the derivation of the DLF and the equivalent SDOF systems can be found in Biggs [1964]. A SDOF model is based on the assumption that the dynamic response of the structure or structural component is mainly determined by a single, dominant response mode. P-I diagrams for SDOF systems depend on the natural frequency of the system, the defined damage criterion, the pulse shape, and the material behaviour.

The influence of the pulse shape on the P-I diagram for a linear-elastic SDOF system was investigated in Li and Meng [2002a] and for an elastic-plastic SDOF system in Li and Meng [2002b]. Elastic-plastic hardening and softening SDOF systems have also been investigated recently by Fallah and Louca [2007]. Most investigations only consider decaying idealized blast loads (pulse shapes that begin with maximum pressure). For these types of pulse shape, the SDOF P-I diagram has a hyperbolic shape. Pulse shapes with finite rise time result in P-I diagrams that are not of a hyperbolic shape, as shown in Smith and Hetherington [1994]. When the material behaviour and the pulse shape become too complex for an analytical solution, P-I diagrams can be derived numerically, as described by Krauthammer et al. [2008]. It can be concluded that P-I diagrams are generally derived from equivalent SDOF systems, which are deduced from structural components (or structures). Since the influence of higher modes is ignored in these systems, it is expected that the P-I diagrams will fail to predict behaviour of the actual structure, when it is loaded in the impulse regime.

In Karthaus and Leussink [1983], the importance of the higher modes for the dynamic response is shown for a simply supported beam subjected to a uniformly distributed load. The necessity of taking shear deformation and rotary inertia into account when higher modes are important, is also demonstrated. In text books on the subject of blast loaded structures (such as Bangash [1993], Smith and Hetherington [1994] and Kappos [2002]) as well as design manuals (such as for example the design manual of the US Army, Navy and Air Force [1990]), the consequences of neglecting higher modes in constructing P-I diagrams

are not sufficiently emphasized. Only in VROM [2003] the applicability of P-I diagrams is limited to $t_d/T_1 > 0.1$ (blast duration / first natural period) and a uniform load distribution.

In Shi et al. [2008], P-I diagrams are determined for reinforced concrete columns subjected to blast loads using the program LS-DYNA, including higher modes, elastic-plastic hardening, and strain rate effects. A comparison is made with the SDOF approach of Fallah and Louca [2007], which includes neither strain rate effects, nor higher modes. Therefore it is unclear whether the differences between the results from these two approaches are caused by strain rate effects, higher modes, or both. Furthermore, Shi et al. [2008] assume that the shape of the P-I diagram including higher modes is hyperbolic, and this shape is fitted to the data from the finite element (FE) analysis by curve fitting. To separate the influence of the inclusion of higher modes from other influences, this theoretical study investigates the forced dynamic response of a continuous Timoshenko beam in the elastic regime, with and without the inclusion of higher modes. The Timoshenko beam represents a multistory building, and includes shear deformation and rotary inertia. The assumption of linear-elastic material behaviour allows for the use of the mode superposition method to determine the dynamic response. Strain-rate effects are neglected. More information about the derivation of the Timoshenko beam from the multistory building structure can be found in Van der Meer [2008].

The rest of this paper is structured as follows. In Sections 2 and 3 the P-I diagram and the Equivalent SDOF Method (ESM) are introduced. In Section 4, the mode shapes and natural frequencies are derived according to Han et al. [1999], and forced response is treated in Section 5. Modal contribution factors for base shear and base moment are obtained in Section 6, by adapting a method described in Chopra [1995] for earthquake engineering. The determination of dynamic response including higher modes, using these modal contribution factors, is referred to as the Modal Contribution Factor Method (MCFM). In Section 7, this method is compared to the Equivalent SDOF Method. Instead of the maximum transverse deflection, which is commonly used to determine P-I diagrams for equivalent SDOF systems, the maximum dynamic base shear is used to define the P-I diagram, *including higher modes*, in Section 8. Approximation of the asymptotes of the P-I diagram, as well as the influence of slenderness and spatial load distribution on these asymptotes, are also discussed in this section. Assumptions, on which the results in this paper are based, are given in Section 9. A discussion, conclusions and recommendations for further research are given in Sections 10, 11 and 12 respectively.

2 Introduction to P-I diagrams

Much information about P-I diagrams can be found in the references given in the introduction. In spite of this, a short introduction to the pressure-impulse diagram will be given in this section. The term *pressure-impulse diagram* is somewhat misleading, because it is also used in literature for load-impulse diagrams. However, the principle of both diagrams is the same. The diagram determined in this paper is a dimensionless load-impulse diagram, which is shown schematically in Figure 1.

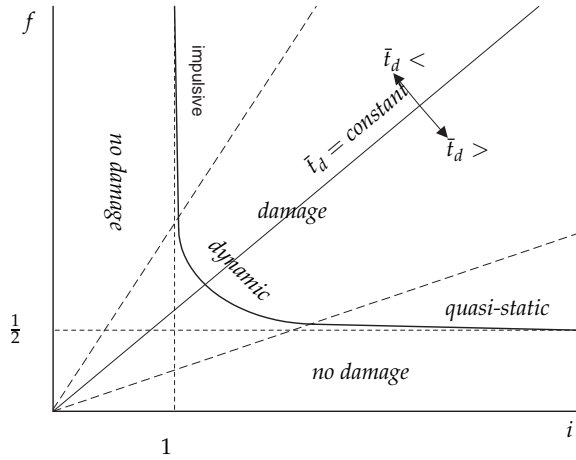


Figure 1: Schematic $f - i$ -diagram for pulse shapes with maximum at $t = 0$

If f is the dimensionless load, then the dimensionless impulse i , which is the area of the pulse shape, can be written as $\beta f \bar{t}_d$ for any pulse shape, in which $\bar{t}_d = \omega_1 t_d$ is the dimensionless blast duration. β is a pulse shape factor between 0 and 1 ($\beta = 1$ indicates a rectangular pulse shape, and $\beta = 1/2$ a triangular pulse shape). ω_1 is the first natural frequency in rad/s. For a given pulse shape, every \bar{t}_d value corresponds to a straight line through the origin of the $i - f$ -plane. On each of these lines, three of which are given in Figure 1, a point can be obtained by equating the maximum dynamic response and the defined damage criterion. All these points together define the $f - i$ -diagram.

The maximum dynamic SDOF response is $r_{dyn} = r_{st} \bar{D}_{1,max}$, in which r_{st} is the static response, and $\bar{D}_{1,max}$ is the first maximum of the time-dependent dynamic load factor $\bar{D}_1(\bar{t})$ (which is given in (13) for the pulse shape of Figure 4). $\bar{D}_{1,max}$ is called the dynamic load

factor (DLF). If the damage criterion is $r_{dyn} = r_c$, in which r_c is the critical response, then

$$\frac{r_{dyn}}{r_c} = \frac{r_{st}\bar{D}_{1,max}}{r_c} = 1 \quad \rightarrow \quad \frac{r_{st}}{r_c} = \frac{1}{\bar{D}_{1,max}} = f \quad (1)$$

The dynamic load factor $\bar{D}_{1,max}$, is a function of the dimensionless blast duration \bar{t}_d , and depends on the pulse shape. The static response r_{st} depends only on the applied load, hence the dimensionless load can be defined as $f = r_{st}/r_c$.

The area left and below the curve, which defines the $f - i$ -diagram, gives all possible combinations of f and i for which the damage criterion is not exceeded (*no damage*). The area right and above the curve, gives all possible combination of f and i for which the damage criterion is exceeded (*damage*). *Damage* and *no damage* areas are given in Figure 1. In literature, P-I-diagrams are sometimes referred to as iso-damage curves, because several curves can be drawn in the same diagram to represent different damage levels.

Since $\bar{t}_d = \omega_1 t_d = 2\pi t_d/T_1$, the dimensionless blast duration \bar{t}_d is proportional to the ratio of the blast duration t_d and the fundamental natural period T_1 of the structure. For low values of t_d/T_1 , the response equals impulse response, so $\bar{D}_{1,max} = \bar{t}_d/2$ and $i = 1$, which is called the *impulse* asymptote. For high values of t_d/T_1 , the pulse shape approaches a step force (if the pulse shape has its maximum at $t = 0$), for which $\bar{D}_{1,max} = 2$ and $f = 1/2$, which is called the *quasi-static* asymptote. If $t_d/T_1 \approx 1$, the response is neither impulse nor quasi-static, and this is called the *dynamic* regime. The three regimes of the $f - i$ -diagram, *impulse*, *quasi-static* and *dynamic*, are given in Figure 1. The $f - i$ -diagram in this section is typical for SDOF response. Numerical determination of a $f - i$ -diagram including higher modes is treated in Section 8.

3 Introduction to the Equivalent SDOF Method

The Equivalent SDOF Method can be found in for example Biggs [1964]. As an introduction to Section 7 a short explanation of the Equivalent SDOF Method is given here. The method is based on energy equivalence between the continuous beam, as shown in Figure 2a, and an equivalent SDOF spring-mass system, as shown in Figure 2b. In Figure 2a, H is the height of the beam in x -direction, $P(x, t)$ is the load distribution over the beam, $y(x, t)$ is the transverse deflection of the beam, EI is the bending stiffness, GA is the shear stiffness, m is the beams mass per unit length, and x is the axial coordinate of the beam from clamped to free end. In Figure 2b, K_{eq} is the equivalent stiffness, M_{eq} is the equivalent mass, $F_{eq}(t)$ is the equivalent load, and $y(t)$ is the displacement (degree of freedom or DOF).

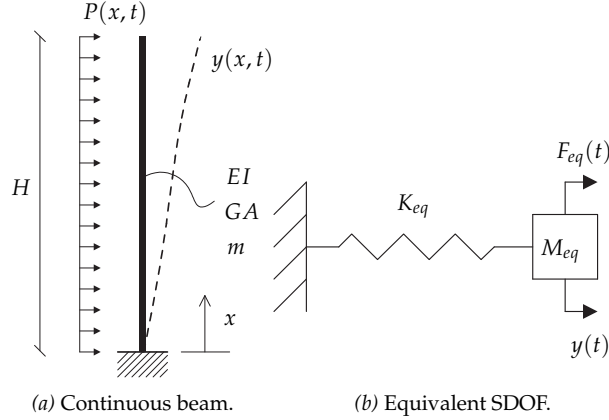


Figure 2: Equivalent SDOF Method

The equivalent SDOF systems has the following properties:

$$y = \frac{F_{eq}}{K_{eq}} \quad \omega_1 = \sqrt{\frac{K_{eq}}{M_{eq}}} \quad y(t) = y\bar{D}_1(t) \quad (2)$$

in which ω_1 is the first natural frequency in rad/s, and $\bar{D}_1(t)$ is the time dependent dynamic load factor, which is dependent of the pulse shape, the blast duration t_d , and the natural frequency ω_1 . The equivalent mass M_{eq} is determined by equating kinetic energy of both systems, the equivalent load F_{eq} is obtained by equating work done in both systems, and the equivalent stiffness K_{eq} is obtained by equating strain energy of both systems. The time variation of the force and displacement is assumed to be similar for both systems. Hence it can be ignored in these equations. To be able to determine the equivalent mass, load and stiffness, a shape function $y(x)$ should be chosen for the beam, and this shape function should be related to the displacement y of the equivalent SDOF system. Usually the maximum deflection is chosen as the degree of freedom, so that $y = y(H)$ for a cantilevered beam.

The shape function $y(x)$ should satisfy the boundary conditions of the beam. Two shape functions that satisfy these conditions are the static deflected shape $y_{st}(x)$ due to the load $P(x)$, and the dynamic deflected shape in the first mode $y_1(x)$, which is the first mode shape multiplied by a constant. If $y_{st}(x)$ is used, the static deflection of the equivalent SDOF system is exact, but the natural frequency is overestimated. Since $y_{st}(x)$ depends on the load distribution $P(x)$, the natural frequency ω_1 would also depend on $P(x)$, which is incorrect. On the other hand, if $y_1(x)$ is used, the natural frequency of the equivalent SDOF system is exact, but the static deflection is approximated, because $y_1(x)$ is an approximation

of $y_{st}(x)$ for all but one unique load distribution. For non-uniform load distributions, $y_{st}(x)$ and $y_1(x)$ differ more than for a uniform load distribution. For this reason, only uniform load distribution is allowed in VROM [2003].

The consequences of the selected shape function for the P-I diagram are as follows. If $y_{st}(x)$ is used, the impulse asymptote is approximated, because it is governed by ω_1 , which is overestimated. If $y_1(x)$ is used, the quasi-static asymptote is approximated, because it is governed by the static deflection. The equivalent SDOF system only yields exact results when $y_1(x)$ and $y_{st}(x)$ are equal, which is only true for one specific load distribution $P(x)$. For all other load distributions, higher modes have contributions to the response. This is one of several reasons to take into account the influence of higher modes.

4 Mode shapes and natural frequencies of a transversely vibrating cantilevered Timoshenko beam

The mode shapes of a transversely vibrating clamped-free Timoshenko beam, which includes shear deformation and rotary inertia, are derived according to Han et al. [1999]. The beam is shown in figure 2a. Mode shapes and natural frequencies of a Timoshenko beam are dependent on a geometry parameter s and a material parameter γ . These are defined as

$$s = H\sqrt{\frac{A}{I}} \quad (3)$$

$$\gamma = \sqrt{\frac{E}{G}} \quad (4)$$

in which A is the area of the beam cross section, I is the second moment of area of the beam cross section, E is the Young's modulus, and G is the shear modulus.

The Timoshenko beam has two dependent mode shapes for every n^{th} mode, namely $W_n(x)$, which is the transverse deflection of the n^{th} mode including shear deflection, and $\Psi_n(x)$, which is the rotation due to bending moment of the n^{th} mode. The mode shapes are given in dimensionless form with $\bar{x} = x/H$ and $\bar{W}_n = W_n/H$. Ψ_n is in radians and thus dimensionless.

The mode shapes are functions of the dimensionless wave numbers a_n and b_n , which depend on s and γ , and are the solution sets of the frequency equation. The frequency equation is dependent on the boundary conditions of the Timoshenko beam. For a

cantilevered Timoshenko beam, the frequency equation is given in Han et al. [1999] by

$$a_n b_n \frac{(a_n^2 - b_n^2) \sin a_n \sinh b_n - (a_n^4 + a_n^4 \gamma^4 + 4\gamma^2 a_n^2 b_n^2 + b_n^4 \gamma^4 + b_n^4)}{(b_n^2 + \gamma^2 a_n^2)(a_n^2 + \gamma^2 b_n^2)} \cos a_n \cosh b_n - 2a_n b_n = 0 \quad (5)$$

The mode shapes are given by

$$\begin{aligned} \Psi(\bar{x}) = & C_n \left(\sin a_n \bar{x} + \frac{a_n(b_n^2 + \gamma^2 a_n^2)}{b_n(a_n^2 + \gamma^2 b_n^2)} \sinh b_n \bar{x} \right. \\ & + \frac{a_n \cos a_n + \frac{a_n(b_n^2 + \gamma^2 a_n^2)}{a_n^2 + \gamma^2 b_n^2} \cosh b_n}{a_n \sin a_n + b_n \sinh b_n} \\ & \left. (\cos a_n \bar{x} - \cosh b_n \bar{x}) \right) \end{aligned} \quad (6)$$

and

$$\begin{aligned} \bar{W}_n(\bar{x}) = & C_n \left(\left[\frac{(1 + \gamma^2)a_n}{a_n^2 + \gamma^2 b_n^2} \sin a_n \bar{x} - \frac{(1 + \gamma^2)b_n}{b_n^2 + \gamma^2 a_n^2} \sinh b_n \bar{x} \right] \right. \\ & + \frac{a_n \cos a_n + \frac{a_n(b_n^2 + \gamma^2 a_n^2)}{a_n^2 + \gamma^2 b_n^2} \cosh b_n}{a_n \sin a_n + b_n \sinh b_n} \\ & \left. + \frac{(1 + \gamma^2)a_n}{a_n^2 + \gamma^2 b_n^2} (\cosh b_n \bar{x} - \cos a_n \bar{x}) \right) \end{aligned} \quad (7)$$

If a_n is larger than a critical wave number a_c , b_n should be replaced by $j b_n$, with $j^2 = -1$.

The critical wave number is

$$a_c = s \sqrt{\frac{1}{\gamma^2} + 1} \quad (8)$$

For a given s and γ , the mode shapes can be determined except for the constant C_n . This constant can be determined by ortho-normalizing the mode shapes with respect to each other, using

$$\int_0^1 \left(\bar{W}_n(\bar{x}) \bar{W}_m(\bar{x}) + \frac{1}{s^2} \Psi_n(\bar{x}) \Psi_m(\bar{x}) \right) d\bar{x} = \delta_{nm} \quad (9)$$

where δ_{nm} is the Kronecker delta, which is 1 for $n = m$ and 0 otherwise.

The dimensionless natural frequency $\bar{\omega}_n = \omega_n / \omega_1$ can be determined as

$$\bar{\omega}_n = \sqrt{\frac{a_n^2 - b_n^2}{1 + \gamma^2}} \sqrt{\frac{s^2}{\bar{m}}} \quad \text{and if } a_n > a_c, b_n \rightarrow j b_n \quad (10)$$

in which $\bar{m} = mH^4 \omega_1^2 / EI$. For $\gamma = \sqrt{2.6}$ (steel), $s = 6.66$, $EI = 5.16 \cdot 10^{11} \text{ Nm}^2$, $H = 64.8 \text{ m}$ and $m = 31778 \text{ kg/m}$, representing a trussed frame load-bearing element of a building

Mode	a_n	b_n	$\bar{\omega}_n$	C_n
1	1.84075	1.62824	1.000000	0.456837
2	4.14219	2.52714	3.817710	0.297457
3	7.07301	1.63825	8.003859	0.165948
4	8.69907	1.94629	10.36927	0.146420
5	10.83199	4.07270	13.46139	0.179251
6	11.67560	4.78576	14.67817	0.198263
7	14.27275	6.81980	18.40055	0.098236
8	15.40061	7.65717	20.00672	0.187232
9	17.58377	9.22948	23.10053	0.076141
10	19.49123	10.56530	25.78965	0.125137

Table 1: Wave number and frequencies for a Timoshenko beam with $\gamma^2 = 2.6$, $s = 6.66$, $EI = 5.16 \cdot 10^{11} \text{Nm}^2$, $H = 64.8\text{m}$ and $m = 31778\text{kg/m}$

structure, the wave numbers, natural frequencies and constants C_n for the first 10 modes are tabulated in Table 1. The horizontal line between mode 3 and 4 indicates the critical wave number a_c . With the parameters from Table 1, the mode shapes \bar{W}_n and Ψ_n can be drawn, which is done in Figure 3a and 3b respectively, for the first four modes.

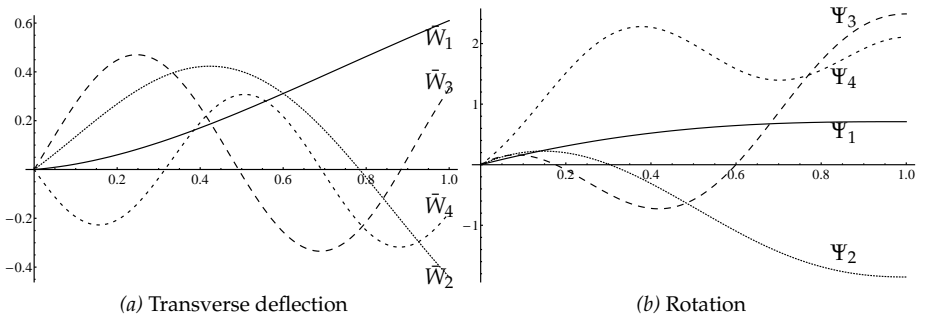


Figure 3: First four mode shapes of cantilevered Timoshenko beam with $s=6.66$ and $\gamma^2=2.6$

5 Forced response of a Timoshenko beam using mode superposition

The mode shapes and natural frequencies depend only on geometry and material parameters and are independent of the applied dynamic load. The forced response of a Timoshenko beam depends both on the mode shapes and natural frequencies, and on the

applied dynamic load. This load has a spatial distribution $\bar{P}(\bar{x})$, and a time distribution $\bar{F}(\bar{t})$. In this paper, it is assumed that $\bar{P}(\bar{x})$ is uniformly distributed, unless reported otherwise, and that $\bar{F}(\bar{t})$ is a linear decaying idealized blast load. Thus

$$\bar{P}(\bar{x}) = \bar{P}_m = \frac{P_m H^3}{EI} \quad (11)$$

in which P_m is a line load in N/m and \bar{P}_m its dimensionless equivalent, and

$$\bar{F}(\bar{t}) = \left(1 - \frac{\bar{t}}{\bar{t}_d}\right) [u(\bar{t}) - u(\bar{t} - \bar{t}_d)] \quad (12)$$

in which $u(\bar{t} - \bar{t}_d)$ is a unit step function, t_d is the duration of the blast, and t the time in seconds. Dimensionless equivalents of t_d and t are $\bar{t} = \omega_1 t$ and $\bar{t}_d = \omega_1 t_d$. The time distribution is shown in Figure 4.

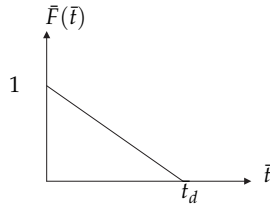


Figure 4: Idealized blast load, force-time profile or pulse shape

Each mode responds as a SDOF system. The time dependent dynamic load factor $\bar{D}_n(\bar{t})$ is determined by the natural frequency $\bar{\omega}_n$, the duration of the blast \bar{t}_d and the pulse shape. The time dependent dynamic load factor for the blast shown in Figure 4 is given in Biggs [1964]:

$$\bar{D}_n(\bar{t}) = \begin{cases} -\frac{\bar{t}}{\bar{t}_d} + 1 - \cos \bar{\omega}_n \bar{t} + \frac{\sin \bar{\omega}_n \bar{t}}{\bar{\omega}_n \bar{t}_d} & \text{if } \bar{t} \leq \bar{t}_d \\ -\cos \bar{\omega}_n \bar{t} + \frac{\sin \bar{\omega}_n \bar{t}}{\bar{\omega}_n \bar{t}_d} - \frac{\sin \bar{\omega}_n (\bar{t} - \bar{t}_d)}{\bar{\omega}_n \bar{t}_d} & \text{if } \bar{t} > \bar{t}_d \end{cases} \quad (13)$$

The first maximum of $\bar{D}_1(\bar{t})$ is the dynamic load factor (DLF) of a SDOF system.

The dynamic response in the n^{th} mode is a product of the time dependent dynamic load factor $\bar{D}_n(\bar{t})$, the mode shape $\bar{W}_n(\bar{x})$ and the modal participation factor, which is

$$\bar{F}_n = \int_0^1 \bar{W}_n(\bar{x}) \bar{P}(\bar{x}) d\bar{x} \quad (14)$$

The modal participation factor and its derivation can be found in, for example, Thomson [1988]. Although it allows to compare contributions of mode shapes to the response, for a certain dynamic load, it does not give information about the relative contribution of a mode to the total response.

The dynamic transverse displacement $\bar{y}_n(\bar{x}, \bar{t})$, rotation $\varphi(\bar{x}, \bar{t})$, moment $\bar{\mu}_n(\bar{x}, \bar{t})$ and shear force $\bar{v}_n(\bar{x}, \bar{t})$ in the n^{th} mode are determined according to Han et al. [1999] and Chopra [1995] as

$$\bar{y}_n(\bar{x}, \bar{t}) = \frac{\bar{F}_n}{\bar{\omega}_n^2} \bar{D}_n(\bar{t}) \bar{W}_n(\bar{x}) \quad (15)$$

$$\varphi_n(\bar{x}, \bar{t}) = \frac{\bar{F}_n}{\bar{\omega}_n^2} \bar{D}_n(\bar{t}) \Psi_n(\bar{x}) \quad (16)$$

$$\bar{\mu}_n(\bar{x}, \bar{t}) = \frac{\bar{F}_n}{\bar{\omega}_n^2} \bar{D}_n(\bar{t}) \frac{d\Psi_n(\bar{x})}{d\bar{x}} \quad (17)$$

$$\bar{v}_n(\bar{x}, \bar{t}) = \frac{\bar{F}_n}{\bar{\omega}_n^2} \bar{D}_n(\bar{t}) \alpha \left(\frac{d\bar{W}_n(\bar{x})}{d\bar{x}} - \Psi_n(\bar{x}) \right) \quad (18)$$

in which $\bar{y}_n = y_n/H$, $\bar{\mu}_n = \mu_n H/EI$, $\bar{v}_n = v_n H^2/EI$ and $\alpha = s^2/\gamma^2 = GAH^2/EI$. The expressions for moment and shear in equations (17) and (18) respectively are difficult to use, since they require derivatives of all mode shapes to be calculated.

6 Modal Contribution Factor Method

In this section, the Modal Contribution Factor Method (MCFM), adapted from Chopra [1995], is introduced. First, alternative expressions for moment and shear (internal forces) are derived according to paragraph 16.6 of Chopra [1995]. Then, internal forces of the beam in the n^{th} mode are determined from the static forces associated with displacements $\bar{y}_n(\bar{x}, \bar{t})$ of equation (15). Subsequently, the spatial equation of dynamic equilibrium is substituted herein to obtain the alternative expression for the internal forces. The method is able to determine internal forces at every location in the beam, but is specialized here for base shear and base moment, because these are normative for cantilevered beams. The *modal contribution factor* is derived for base shear and base moment in Sections 6.1 and 6.2 respectively. If response is determined for a finite number of modes, a correction factor should take into account the neglected higher modes, which is discussed in Section 6.3.

6.1 Base shear

The spatial distribution of internal shear forces in mode n can be expressed as

$$\begin{aligned}\bar{V}_n(\bar{x}) &= \alpha \left(\frac{d^2 \bar{y}_n(\bar{x})}{d\bar{x}^2} - \frac{d\varphi_n(\bar{x})}{d\bar{x}} \right) \\ &= \frac{\alpha \bar{F}_n}{\bar{\omega}_n^2} \left(\frac{d^2 \bar{W}_n(\bar{x})}{d\bar{x}^2} - \frac{d\Psi_n(\bar{x})}{d\bar{x}} \right)\end{aligned}\quad (19)$$

The spatial equation of dynamic equilibrium is given by

$$\alpha \left(\frac{d^2 \bar{W}_n}{d\bar{x}^2} - \frac{d\Psi_n(\bar{x})}{d\bar{x}} \right) = \bar{\omega}_n^2 \bar{m} \bar{W}_n(\bar{x}) \quad (20)$$

Substituting (20) in (19) leads to

$$\bar{V}_n(\bar{x}) = \bar{F}_n \bar{m} \bar{W}_n(\bar{x}) \quad (21)$$

Base shear for mode n is obtained by integrating (21):

$$\bar{v}_{b;n} = \bar{F}_n \bar{m} \int_0^1 \bar{W}_n(\bar{x}) d\bar{x} \quad (22)$$

Base shear response is obtained by multiplying (22) by $\bar{D}_n(t)$ and summing the contributions of all modes:

$$\bar{v}_b(\bar{t}) = \sum_{n=1}^{\infty} \bar{F}_n \bar{m} \bar{D}_n(\bar{t}) \int_0^1 \bar{W}_n(\bar{x}) d\bar{x} \quad (23)$$

The modal contribution factor for base shear is defined as the ratio of base shear in mode n (22) and base shear due to the application of $\bar{P}(\bar{x})$ as a static force:

$$c_{bs;n} = \frac{\bar{F}_n \bar{m} \int_0^1 \bar{W}_n(\bar{x}) d\bar{x}}{\int_0^1 \bar{P}(\bar{x}) d\bar{x}} \quad (24)$$

The modal contribution factors determined by (24) sum up to unity. Hence the number of modes, which need to be taken into account for sufficient accuracy (e.g. 95%), can be determined. The dimensionless dynamic base shear response can be obtained in terms of the modal contribution factors from (23) and (24):

$$\bar{v}_b(\bar{t}) = \bar{v}_{b;st} \sum_{n=1}^{\infty} c_{bs;n} \bar{D}_n(\bar{t}) \quad \text{with} \quad \bar{v}_{b;st} = \int_0^1 \bar{P}(\bar{x}) d\bar{x} \quad (25)$$

Equation (25) separates the static response from the contributions of all modes to the dynamic response, and therefore gives better understanding of higher mode response than equation (23).

6.2 Base moment

The spatial distribution of internal moments in mode n can be expressed as

$$\begin{aligned}\bar{M}_n(\bar{x}) &= \alpha \left(\frac{d\bar{y}_n(\bar{x})}{d\bar{x}} - \varphi_n(\bar{x}) \right) + \frac{d^2\varphi_n(\bar{x})}{d\bar{x}^2} \\ &= \frac{\bar{F}_n}{\bar{\omega}_n^2} \left[\alpha \left(\frac{d\bar{W}_n(\bar{x})}{d\bar{x}} - \Psi_n(\bar{x}) \right) + \frac{d^2\Psi_n(\bar{x})}{d\bar{x}^2} \right]\end{aligned}\quad (26)$$

The spatial equation of dynamic equilibrium is given by

$$\alpha \left(\frac{d\bar{W}_n(\bar{x})}{d\bar{x}} - \Psi_n(\bar{x}) \right) + \frac{d^2\Psi_n(\bar{x})}{d\bar{x}^2} = \bar{\omega}_n^2 \frac{\bar{m}}{s^2} \Psi_n(\bar{x}) \quad (27)$$

Substituting (27) in (26) leads to

$$\bar{M}_n(\bar{x}) = \bar{F}_n \frac{\bar{m}}{s^2} \Psi_n(\bar{x}) \quad (28)$$

Base moment for mode n is obtained by

$$\begin{aligned}\bar{\mu}_{b;n} &= \int_0^1 \bar{M}_n(\bar{x}) d\bar{x} + \int_0^1 \bar{x} \bar{V}_n(\bar{x}) d\bar{x} \\ &= \bar{F}_n \bar{m} \left(\frac{1}{s^2} \int_0^1 \Psi_n(\bar{x}) d\bar{x} + \int_0^1 \bar{x} \bar{W}_n(\bar{x}) d\bar{x} \right)\end{aligned}\quad (29)$$

Base moment response is obtained by multiplying (29) by $\bar{D}_n(t)$, and summing the contributions of all modes:

$$\bar{\mu}_b(\bar{t}) = \sum_{n=1}^{\infty} \bar{F}_n \bar{m} \bar{D}_n(\bar{t}) \left(\frac{1}{s^2} \int_0^1 \Psi_n(\bar{x}) d\bar{x} + \int_0^1 \bar{x} \bar{W}_n(\bar{x}) d\bar{x} \right) \quad (30)$$

The modal contribution factor for base moment is defined as the ratio of base moment in mode n (29) and base moment due to the application of $\bar{P}(\bar{x})$ as a static force:

$$c_{bm;n} = \frac{\bar{F}_n \bar{m} \left(\frac{1}{s^2} \int_0^1 \Psi_n(\bar{x}) d\bar{x} + \int_0^1 \bar{x} \bar{W}_n(\bar{x}) d\bar{x} \right)}{\int_0^1 \bar{x} \bar{P}(\bar{x}) d\bar{x}} \quad (31)$$

The procedures for base shear in Section 8 are applicable for base moment also, in which case $c_{bs;n}$, $\bar{v}_{b;n}$ and $\bar{v}_{b;st}$ should be replaced by $c_{bm;n}$, $\bar{\mu}_{b;n}$ and $\bar{\mu}_{b;st} = \int_0^1 \bar{x} \bar{P}(\bar{x}) d\bar{x}$.

6.3 Correction of modal contribution factors

If the modal contribution factors for the number of modes calculated sum up to $(1 - \varepsilon)$, the static response is underestimated by $\varepsilon \cdot 100\%$. Therefore, the modal contribution factors should be corrected by multiplying with a factor $1/(1 - \varepsilon)$. In Table 2, the modal contribution factors for base shear and base moment are given before and after correction, for the load distribution of (11), and the mode shapes shown in Figure 3a and 3b.

Contribution factor → Mode ↓	As calculated		After correction	
	Shear	Moment	Shear	Moment
1	0.6148	0.9249	0.6356	0.9253
2	0.2335	0.0678	0.2414	0.0678
3	0.0593	0.0098	0.0613	0.0098
4	0.0168	-0.0040	0.0174	-0.0040
5	0.0143	0.0041	0.0148	0.0041
6	0.0078	-0.0033	0.0081	-0.0033
7	0.0097	0.0018	0.0100	0.0018
8	0.0025	-0.0014	0.0026	-0.0014
9	0.0060	0.0012	0.0062	0.0012
10	0.0025	-0.0013	0.0026	-0.0013
Sum	0.9672	0.9996	1.0000	1.0000

Table 2: Modal contribution factors for base shear and base moment

7 Comparison to Equivalent SDOF Method

To clarify the relation between the Modal Contribution Factor Method (MCFM), as described in the previous section, and the Equivalent SDOF Method (ESM), both methods are compared. The maximum transverse deflection (top deflection in case of a cantilever) of an equivalent SDOF system is related to the internal forces by an assumed deflected shape, which is typically either the static deflected shape $\bar{y}_{st}(\bar{x})$ or the dynamic deflected shape in the first mode $\bar{y}_1(\bar{x})$, as described in Section 3. The MCFM, *without correction* and using only the first mode, is equal to the ESM, if $\bar{y}_1(\bar{x})$ is used as the shape function. $\bar{y}_{st}(\bar{x})$ and $\bar{y}_1(\bar{x})$ are almost similar if a uniformly distributed load is applied. For non-uniformly distributed loads however, $\bar{y}_{st}(\bar{x})$ and $\bar{y}_1(\bar{x})$ can differ significantly. When several modes contribute to the response, the deflection is not proportional to the internal forces (shear, moment) as is the case for a single mode. Therefore, the maximum transverse deflection is not a good criterion to determine P-I diagrams including higher modes. This is demonstrated in this section, by comparing both methods with respect to static deflection, static base shear and fundamental natural frequency.

7.1 Static deflection

The ESM, based on the dynamic deflected shape in the first mode $\bar{y}_1(\bar{x})$, and the MCFM, without higher modes, are equal. Deflection at the top is used for comparison, because this

is the common DOF for the ESM. Since $\bar{\omega}_1 = \omega_1 / \omega_1 = 1$, $\bar{y}_1(\bar{x})$ is given by (15) by

$$\bar{y}_1(\bar{x}) = \bar{F}_1 \bar{W}_1(\bar{x}) \quad (32)$$

which is the product of the first mode shape and its modal participation factor. \bar{y}_{st} is the static deflected shape under the load $\bar{P}(\bar{x})$. Static deflection for both shapes is compared in Table 3.

Load distribution	$\bar{y}_{st}(1)$	$\bar{y}_1(1)$	$\left(\frac{\bar{y}_1(1)}{\bar{y}_{st}(1)} - 1 \right) \cdot 100\%$
$\bar{P}(\bar{x}) = \bar{P}_m$	0.112	0.115	+2.68%
$\bar{P}(\bar{x}) = 3\bar{P}_m(\bar{x} - 1)^2$	0.0408	0.0451	+10.54%

Table 3: Influence of shape function on static deflection for the ESM ($\bar{P}_m = 0.725$)

With regard to static deflection, the differences between the shape functions are respectively +2.68% for a uniform load distribution, and +10.54% for a quadratic load distribution. This is conservative, since static deflection is overestimated. However, higher modes have a larger influence on internal forces and reactions than on deflection, which will be shown in the next section.

7.2 Static base shear

Using the static deflected shape $\bar{y}_{st}(\bar{x})$, the base shear response $\bar{v}_{b;st}$ of the equivalent SDOF system is simply

$$\bar{v}_{b;st} = \int_0^1 \bar{P}(\bar{x}) d\bar{x} \quad (33)$$

Using the dynamic deflected shape $\bar{y}_1(\bar{x})$, the base shear response $\bar{v}_{b;1}$ is given by

$$\bar{v}_{b;1} = \bar{F}_1 \bar{m} \int_0^1 \bar{W}_1(\bar{x}) d\bar{x} \quad (34)$$

And

$$\frac{\bar{v}_{b;1}}{\bar{v}_{b;st}} = \frac{\bar{F}_1 \bar{m} \int_0^1 \bar{W}_1(\bar{x}) d\bar{x}}{\int_0^1 \bar{P}(\bar{x}) d\bar{x}} = c_{bs;1} \quad (35)$$

which is the modal contribution factor for the first mode. If the correction factor is applied as in Section 6.3, the base shear in the first mode $\bar{v}_{b;1}$ is set equal to the static base shear $\bar{v}_{b;st}$, because $c_{bs;1} = 1$. In Table 4 static base shear and base shear in the first mode are compared for two load distributions.

Load distribution	$\bar{v}_{b;st}$	$\bar{v}_{b;1}$	$c_{bs;1}$
$\bar{P}(\bar{x}) = \bar{P}_m$	0.725	0.446	0.615
$\bar{P}(\bar{x}) = 3\bar{P}_m(\bar{x} - 1)^2$	0.725	0.183	0.252

Table 4: Influence of shape function on static base shear for the ESM ($\bar{P}_m = 0.725$)

If no correction factor is applied, the static base shear, determined with the MCFM method using the first mode, is underestimated, since the influence of higher modes is ignored. For a uniform load distribution, the contribution of higher modes to static base shear is 38.5%, and for a quadratic load distribution it is even larger, namely 74.8%. So although static deflection is overestimated by using the first mode shape, the base shear is underestimated significantly. This is another reason to include higher modes and to use base shear as a damage criterion instead of top deflection. In Section 8.3, it is shown that dynamic base shear in the impulse regime has even more influence of higher modes.

7.3 Natural frequency

The natural frequency of the equivalent SDOF system is equal for the MCFM and the ESM using $\bar{y}_1(\bar{x})$. If the ESM based on $\bar{y}_{st}(\bar{x})$ is used, the natural frequency depends on the load distribution $\bar{P}(\bar{x})$, which is incorrect. For non-uniform load distributions the natural frequency is overestimated, as shown in Table 5. For a uniform load distribution, the natural frequency is approximated quite well. Since the MCFM method *with correction* is otherwise equal to the ESM based on static deflection, but uses the correct natural frequency, it is not completely energy equivalent. However, when more modes are used in the MCFM, the necessary correction becomes smaller and the response more accurate.

Load distribution	$\omega_{1;st}$	ω_1	$\left(\frac{\omega_{1;st}}{\omega_1} - 1\right) \cdot 100\%$
$\bar{P}(\bar{x}) = \bar{P}_m$	3.017	2.897	+4.14%
$\bar{P}(\bar{x}) = 3\bar{P}_m(\bar{x} - 1)^2$	3.551	2.897	+22.58%

Table 5: Influence of shape function on first natural frequency for the ESM

8 $f - i$ diagram

8.1 Numerical determination of $f - i$ diagram for base shear

The dimensionless load-impulse diagram is derived for base shear, because it is concluded from Table 2 that base shear has more contribution of higher modes than base moment. The dimensionless load and impulse are defined as

$$f = \frac{\bar{v}_{b;st}}{\bar{v}_{b;c}} \quad i = \frac{f\bar{t}_d}{2} = \frac{\bar{v}_{b;st}}{\bar{v}_{b;c}} \cdot \frac{\bar{t}_d}{2} \quad (36)$$

in which f is the dimensionless load, $\bar{v}_{b;st}$ is the dimensionless static base shear as in (33), $\bar{v}_{b;c}$ is the dimensionless critical base shear, and i is the dimensionless impulse. If desired, the dimensionless load and impulse for base moment can be obtained by replacing $\bar{v}_{b;st}/\bar{v}_{b;c}$ by $\bar{\mu}_{b;st}/\bar{\mu}_{b;c}$, in which $\bar{\mu}_{b;st}$ is the dimensionless static base moment as in the denominator of (31) and $\bar{\mu}_{b;c}$ is the dimensionless critical base moment.

The load-impulse diagram can be obtained by demanding that the maximum dynamic base shear response (25) equals the critical base shear. It is assumed that the maximum occurs during the first half period of the first mode ($0 < \bar{t} \leq \pi$), and that later maxima are reduced by damping. The maximum is determined numerically. The damped response can be determined by including modal damping in the time-dependent dynamic load factor. However, this falls outside the scope of this paper. Dimensionless load f and dimensionless impulse i are derived from

$$\frac{\max[\bar{v}_b(\bar{t})]_{\bar{t}=0}^{\bar{t}=\pi}}{\bar{v}_{b;c}} = 1 \quad (37)$$

$$f = \frac{\bar{v}_{b;st}}{\bar{v}_{b;c}} = \frac{1}{\max \left[\sum_{n=1}^{\infty} c_{bs;n} \bar{D}_n(\bar{t}) \right]_{\bar{t}=0}^{\bar{t}=\pi}} \quad (38)$$

$$i = \frac{f\bar{t}_d}{2} = \frac{\bar{t}_d}{2} \cdot \frac{1}{\max \left[\sum_{n=1}^{\infty} c_{bs;n} \bar{D}_n(\bar{t}) \right]_{\bar{t}=0}^{\bar{t}=\pi}} \quad (39)$$

Alternatively, for base moment, the contribution factors $c_{bs;n}$ should be replaced by $c_{bm;n}$.

Both f and i depend on $\bar{\omega}_n$ and \bar{t}_d , because $\bar{D}_n(\bar{t})$ (13) depends on $\bar{\omega}_n$ and \bar{t}_d . For the set of $\bar{\omega}_n$, given in Table 1, and the contribution factors from Table 2, the load f and impulse i can be determined from equations (38) and (39) respectively for a range of \bar{t}_d , resulting in a load-impulse diagram.

An arbitrary number of modes can be taken into account, as long as the contribution factors are corrected to sum up to unity, see Table 6. Static base shear is exact when the correction

factor is applied, but dynamic base shear is approximated and becomes more accurate when more modes are taken into account.

n	1 mode	2 modes	3modes
1	1.0000	0.7247	0.6774
2	-	0.2753	0.2573
3	-	-	0.0653

Table 6: Modal contribution factors for base shear, corrected

8.2 Discussion of results of $f - i$ diagram for base shear

The load-impulse diagram which is obtained from Section 8.1 for 1, 2, 3, 10 and 25 modes, is given in Figure 5. The horizontal or quasi-static asymptote, is barely influenced by the number of modes that are taken into account. The vertical or impulse asymptote on the other hand, is significantly influenced by the inclusion of higher modes, although it does not seem to make much difference whether 2, 3, 10 or 25 modes are used. The difference between the number of modes used is best visible in the dynamic regime between the asymptotes, see Figure 5b. In this particular case, a conservative but accurate approximation of the load-impulse diagram can be obtained by including only 3 modes. Furthermore it is observed that a 2-mode approximation is also conservative but less accurate, and that a 1-mode (SDOF) approximation is not conservative in the impulse regime when $t_d/T_1 = i/(\pi f) < \approx 0.21$ (point of intersection of $f - i$ diagrams for 1 and 25 modes). This indicates that the requirement for $f - i$ diagrams in VROM [2003], namely $t_d/T_1 > 0.1$, may not be stringent enough.

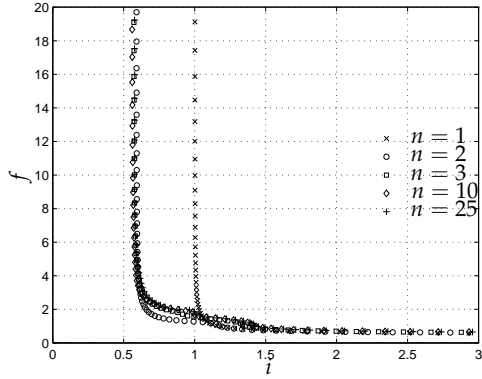
8.3 Approximations of asymptotes of $f - i$ diagram

An approximate P-I diagram including higher modes can be obtained if the quasi-static and impulse asymptotes are known. For the pulse shape shown in Figure 4, the quasi-static asymptote can be determined by replacing $\bar{D}_n(\bar{t})$ in (38) by the response to a step force, which is

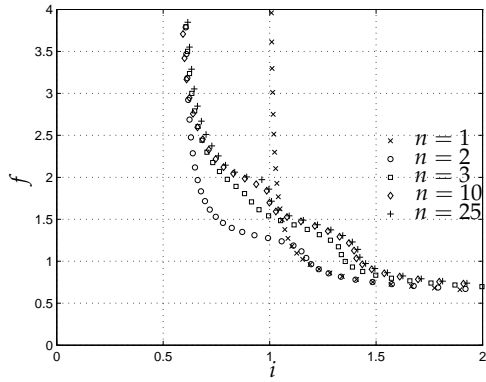
$$\bar{D}_n(\bar{t}) = 1 - \cos \bar{\omega}_n \bar{t} \quad (40)$$

This leads to

$$f = \frac{1}{\max \left[\sum_{n=1}^{\infty} c_{bs;n} (1 - \cos \bar{\omega}_n \bar{t}) \right]_{\bar{t}=0}^{\bar{t}=\pi}} \quad (41)$$



(a) Overview



(b) Detail

Figure 5: Dimensionless load-impulse diagram

The impulse asymptote for any pulse shape can be determined by replacing $\bar{D}_n(\bar{t})$ by the response to an impulse, which is

$$\bar{D}_n(\bar{t}) = \frac{\bar{\omega}_n \bar{t}_d}{2} \sin \bar{\omega}_n \bar{t} \quad (42)$$

Substituting (42) in (39) gives

$$i = \frac{1}{\max \left[\sum_{n=1}^{\infty} c_{bs;n} \bar{\omega}_n \sin \bar{\omega}_n \bar{t} \right]_{\bar{t}=0}^{\bar{t}=\pi}} \quad (43)$$

8.4 Discussion of results for the $f - i$ asymptotes

The contribution of higher modes to the quasi-static response depends on the modal contribution factor $c_{bs;n}$. The contribution of higher modes to the impulse response depends on the product of the modal contribution factor and the dimensionless natural frequency $c_{bs;n}\bar{\omega}_n$. Therefore, impulse response has more contribution from higher modes than quasi-static response. This is shown in Figure 6.

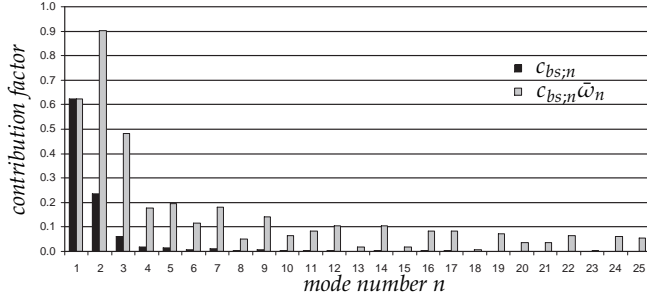


Figure 6: Modal contributions for impulse and quasi-static response for 25 modes

From (41), it is clear that the SDOF quasi-static asymptote is a lower bound for any higher number of DOF, because in this case, $c_{bs;1} = 1$, and the maximum of (40) is 2. When higher modes are included, the maxima of $\bar{D}_n(t)$ are still 2 for every mode, and $\sum_{n=1}^{\infty} c_{bs;n} = 1$, but the total maximum, which is the denominator in (41), is slightly lower than 2 due to interactions of the cosine functions. On the other hand, the SDOF impulse asymptote is an upper bound for any higher number of DOF, because $c_{bs;1}\bar{\omega}_1 = 1$ ($\bar{\omega}_1 = 1$ by definition) and $\max(\sin \bar{\omega}_1 \bar{t}) = 1$. The influence of the higher modes is increased significantly in the impulse regime due to the presence of $\bar{\omega}_n$ in (43). Due to $\bar{\omega}_n$, $\sum_{n=1}^{\infty} c_{bs;n}\bar{\omega}_n \gg 1$, although the total maximum, which is the denominator in (43), is decreased slightly by the interactions of the sine functions.

Technically, the impulse asymptote is not an asymptote, because $\sum_n c_{bs;n}\bar{\omega}_n$ does not converge. Therefore, infinite modes should be taken into account to determine the impulse asymptote. However, it should be noted that, for practical blast loads on structures or components, higher modes from a certain mode onwards are not in the impulse regime. For example, for 25 modes of the Timoshenko beam in this paper, the dynamic load factors $\bar{D}_{n,max}$ are given in Figure 7 versus $\omega_n t_d$, for $t_d = 20$ ms, which is a realistic blast load duration. It can be seen that modes 10-25 deviate from the impulse asymptote. This trend would continue if more modes were included. So, although the first 10 modes are in the

impulse regime, there are higher modes which are not. Since there are infinite modes, there are always higher modes not in the impulse regime. These higher modes have generally low contribution factors and lower $\bar{D}_{n,max}$ than predicted by (42), hence their contribution can be neglected. Consequently, the infinite sum in (43) can be truncated at $n = N$ depending on the duration of the pulse \bar{t}_d compared to the natural frequency $\bar{\omega}_n$ of the mode. The impulse asymptote should also be truncated at the lowest \bar{t}_d value which is deemed realistic for building practice.

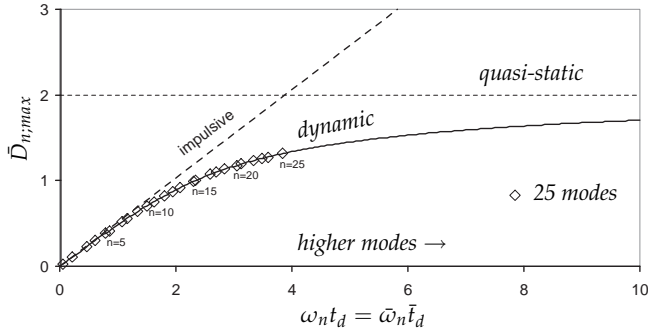


Figure 7: Dynamic load factor: actual vs impulse for 25 modes, $t_d = 20$ ms

The asymptotes, from equations (41) and (43), were evaluated numerically for 1, 2, 3, 10 and 25 modes. The results are shown in Table 7. The quasi-static asymptote of the SDOF case is conservative and can be maintained. The SDOF impulse asymptote is not conservative. The addition of one extra mode shape and natural frequency is already a large improvement compared to SDOF. The numerical values as shown in Table 7 depend on the distribution of contribution factors and natural frequencies. The contribution factors are determined by the spatial distribution of the load and the mode shapes. Mode shapes and natural frequencies depend on material and geometrical properties of the (Timoshenko) beam and on the boundary conditions.

8.5 Influence of load distribution on $f - i$ diagram

Using 10 modes, the impulse asymptote of the $f - i$ diagram was 55.6% of the SDOF impulse asymptote, for a uniform load distribution. For a quadratic load distribution, as in Table 3, the $f - i$ diagram, determined using the method of Section 8.1, is shown in Figure 8. 25 modes were taken into account. The impulse asymptote is reduced to 22% of the SDOF asymptote (see Table 9). From the intersection of the $f - i$ diagrams of 1 and 25 modes, it is

Number of modes	f	i
1	0.5000	1.0000
2	0.5367	0.5899
3	0.5432	0.5711
10	0.5530	0.5573
25	0.5580	0.5720

Table 7: Asymptotes of $f - i$ -diagram including higher modes

Mode number n	$s = 33.3175$	$s = 6.6635$
1	0.613	0.615
2	0.192	0.233
3	0.067	0.059
4	0.035	0.017
5	0.022	0.014

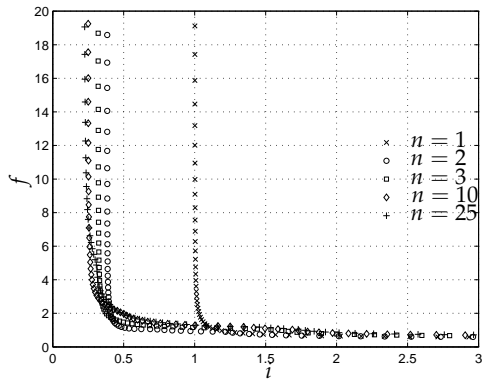
Table 8: Contribution factors for base shear, influence of slenderness

concluded that the SDOF diagram is non-conservative for $t_d/T_1 = i/(\pi f) < \approx 0.26$.

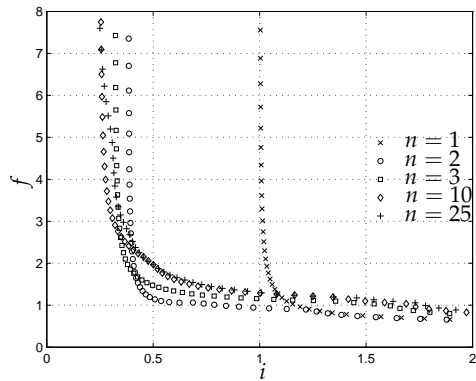
8.6 Influence of slenderness on $f - i$ diagram

The $f - i$ diagrams in the previous sections were determined for a cantilevered Timoshenko beam with a particular slenderness. To gain insight in the behaviour of Euler-Bernoulli beams and more slender Timoshenko beams, the natural frequencies and contribution factors for 25 modes were compared for three Timoshenko beams and one Euler-Bernoulli beam. It was found, that the most significant contribution factors are only slightly influenced by the slenderness, as shown in Table 8, while the natural frequencies for the higher modes increase faster for slender beams, as demonstrated in Figure 9.

Finally, the $f - i$ diagram for $s = 33.3175$ (5 times the original slenderness), is shown in Figure 10. The combined effects of a quadratic load distribution and an increased slenderness are shown in Figure 11. The impulse asymptote is reduced to 14% and 5% of the SDOF asymptote respectively, as shown in Table 9. From the intersection of the $f - i$ diagrams of 1 and 25 modes, it is concluded that the SDOF diagram is non-conservative for $t_d/T_1 = i/(\pi f) < \approx 0.18$ and $t_d/T_1 < \approx 0.48$, for the $f - i$ diagrams of Figure 10b and 11b.



(a) Overview



(b) Detail

Figure 8: Dimensionless load-impulse diagram, quadratic load distribution

9 Assumptions

Before conclusions are drawn, the assumptions, on which the results in this paper are based, are summarized below:

- A cantilevered (clamped-free) Timoshenko beam was investigated, which represents a building structure that exhibits bending and shear deformation.
- Linear-elastic material behaviour was assumed until failure (no ductility), which enabled the use of the mode superposition method.
- The failure criterion was assumed to be independent of the strain rate.

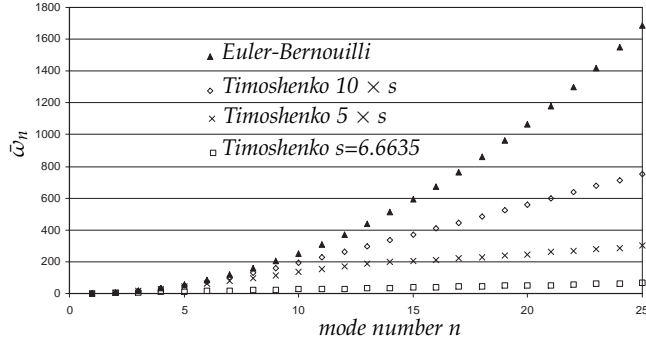


Figure 9: Natural frequencies, influence of slenderness

Method	Load distribution	Slenderness s	f	i
ESM	any	any	0.5000	1.0000
MCFM	$\bar{P}(\bar{x}) = \bar{P}_m$	6.6635	0.5580	0.5720
		33.3175	0.5586	0.1437
	$\bar{P}(\bar{x}) = 3\bar{P}_m(\bar{x} - 1)^2$	6.6635	0.5887	0.2219
		33.3175	0.5888	0.0541

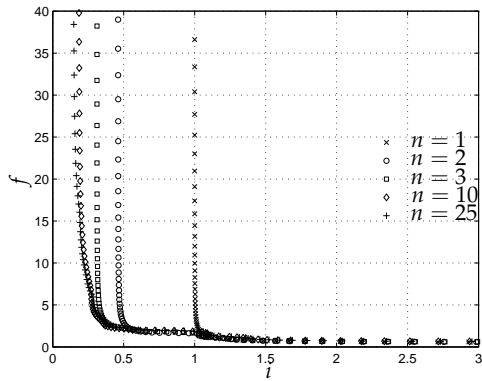
Table 9: Influence of load distribution and slenderness on asymptotes of $f - i$ diagram

- The pulse shape (load-time history) was assumed as given in Figure 4.
- Maximum response was assumed to occur within the first half period of the first mode.
- Damping was neglected in the calculation, but implicitly sufficient damping was assumed, to assure the previous assumption.

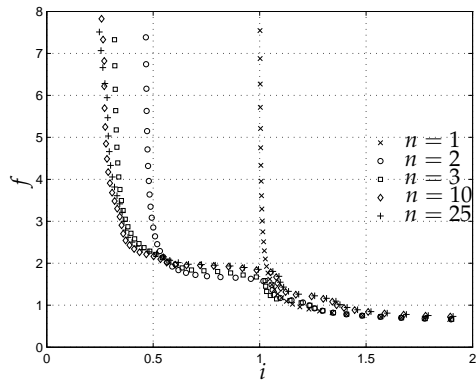
10 Discussion

The theoretical study in this paper has focused on the influence of higher modes on the P-I diagram, without considering strain rate effects and non-linear material behaviour (ductility). Comparison of the ESM (SDOF) and the MCFM (including higher modes) showed that:

- The impulse asymptote of the ESM is non-conservative. Moreover, it is not technically an asymptote.
- The shape of the P-I diagram including higher modes deviates significantly from the



(a) Overview



(b) Detail

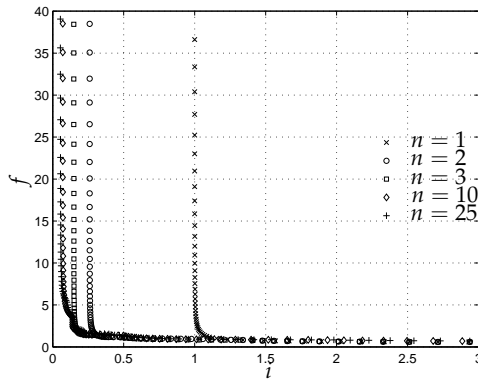
Figure 10: Dimensionless load-impulse diagram, uniform load distribution, $s = 33.3175$

hyperbolic shape of the SDOF P-I diagram, most noticeably in the dynamic regime.

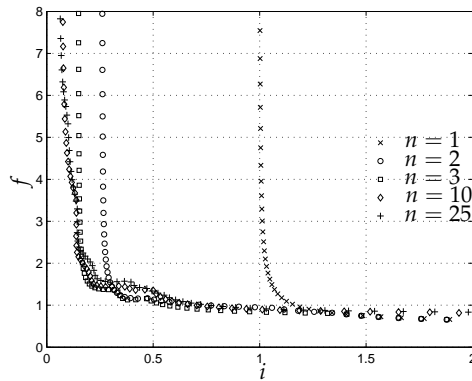
- The quasi-static asymptote of the SDOF P-I diagram is conservative.

However, two main aspects that influence the response to blast loading were neglected in this paper, namely strain rate effects and ductility. Consequences of these and other assumptions, which have been described in Section 9, are evaluated here.

- A cantilevered (clamped-free) Timoshenko beam was investigated, representing a building structure. However, building components, for which P-I diagrams are generally used, have different boundary conditions and slenderness. It is expected



(a) Overview



(b) Detail

Figure 11: Dimensionless load-impulse diagram, quadratic load distribution, $s = 33.3175$

that the MCFM will give similar results for Timoshenko beams with different boundary conditions. It has been demonstrated in this paper, that the influence of higher modes increases with increasing slenderness of the beam, and is highest for Euler-Bernoulli beams.

- Linear-elastic material behaviour was assumed, but response of building components to blast loading will generally be non-linear. Non-linear material behaviour (plasticity, ductility) is difficult to take into account in higher mode response. As a damage criterion, the plastic moment and shear capacity could be applied. However, the formation of plastic hinges changes the mode shapes, until enough hinges are formed for a failure mechanism. Neglecting ductility, as in this

paper, is over-conservative.

- The strain-rate effect, which was neglected in this paper, is expected to have a significant influence on the response to blast loading. For structural steel, the yield and ultimate strength are increased at increased strain rates, but the ductility is decreased. Higher modes respond faster than the first mode and therefore cause higher strain rates. In the impulse regime, where the higher modes have a significant influence on the response, strain rate effects are expected to be more important than ductility. In the quasi-static regime, where higher modes contribute less to the response, it is expected that ductility is more important. Both strain rate effects and ductility increase the damage criterion, so neglecting these aspects is over-conservative. It would be interesting, as a next step, to investigate linear-elastic behaviour in combination with strain rate effects, using the method of this paper. These results could be compared to a FE analysis which also includes non-linear material behaviour, such as Shi et al. [2008].
- The pulse shape (load-time history) was assumed as given in Figure 4. The impulse and quasi-static asymptotes are not affected by the pulse shape (if maximum load occurs at $t = 0$). Therefore, the selected pulse shape is of minor importance.
- The maximum response was assumed to occur within the first half period of the first mode. In the quasi-static and dynamic regime, for decaying blast loads, this is true because the maximum response is governed by the load, which is maximal at $t = 0$. The maximum response occurs during or close to the forced vibration part of the response. In the impulse regime, the maximum response is governed by the impulse and the maximum response occurs during the free vibration part of the response, which is a sum of sine functions as shown in the denominator of (43). Since the period of this response is much larger than the first mode period T_1 , the maximum of undamped response can occur after $t = T_1$. Therefore, sufficient damping has to be assumed to reduce peaks that occur after $t = T_1$.
- Damping was neglected in the calculations, but implicitly enough damping was assumed, to ensure that the maximum response occurred within the first half period of the first mode ($0 \leq t \leq T_1/2$). This assumption is only needed in the impulse regime. Since response in the impulse regime is governed by higher modes, which are damped faster than the first mode, this assumption was deemed acceptable.

11 Conclusions

- A Modal Contribution Factor Method, which takes into account the influence of higher modes on P-I diagrams for blast loading, was developed in this paper, based on Chopra [1995] and Han et al. [1999]. The method uses mode superposition, which requires linear-elastic material behaviour and knowledge of the mode shapes and natural frequencies. Strain-rate effects are neglected.
- Modal contributions factors for base shear and base moment were derived, which represent the contribution of a mode to the total base shear or total base moment in percent. This enables the user to assess which modes need to be taken into account.
- For the linear-elastic cantilevered Timoshenko beam, the shape of the P-I diagram including higher modes deviates significantly from the hyperbolic shape of the SDOF P-I diagram. Technically, there is no impulsive asymptote.
- For the linear-elastic cantilevered Timoshenko beam, the response in the impulse and dynamic regime is underestimated by the Equivalent SDOF Method.

12 Recommendations

- P-I diagrams to assess response of building structures to blast loading are only valuable when the building facade remains intact. It is likely that building components will fail before the building structure does, because they respond faster. Therefore, building components should be assessed before assessing the building structure as a whole.
- For engineering practice, the advice is to apply the Equivalent SDOF Method and P-I diagrams resulting from it, with great care, especially for $t_d/T_1 \leq 0.2$ and for non-uniform spatial blast load distributions. If the mode shapes are known, the contribution factors can be determined for a specific spatial load distribution, to assess the influence of higher modes. The MCFM can also be adapted for discrete finite element (FE) models, using matrix notation. The modal contribution factors can then be determined, after the mode shapes have been obtained by modal analysis with a FE program.
- The possibility to include the strain-rate effect in the Modal Contribution Factor Method by coupling damage criterion (failure at yield stress) and strain rate should be investigated. By comparison with finite element analysis, such as Shi et al. [2008], the separate effects of strain rate and non-linear material behaviour, could be made

clear. For materials such as structural steel, with increased strength but decreased ductility at high strain rates, it might be possible to accurately approximate the asymptotes of the P-I diagram. The quasi-static asymptote may be approximated with the ESM including an average strain rate effect and non-linear material behaviour, while the impulsive asymptote may be determined with the MCFM, including higher modes and strain rate effects, but excluding non-linear material behaviour.

- Linear-elastic material behaviour is unrealistic for response to blast loading. When material behaviour is non-linear and higher modes and strain rate effects have to be included, non-linear FE simulations, such as Shi et al. [2008], may be the only option. The shape of the P-I diagram should result directly from these simulations, instead of assuming a hyperbolic shape.
- The boundary conditions chosen in this paper (clamped-free) were based on a building structure as a whole. Other boundary conditions such as hinged-hinge and clamped-clamped, which are more common for structural components, should be investigated. Also the influence of an axial load should be taken into account, to extend the problem to columns. Shear deformation and rotary inertia should be included.

References

- G. R. Abrahamson and H. E. Lindberg. Peak load-impulse characterization of critical pulse loads in structural dynamics. *Nuclear Engineering and Design*, 37:35–46, January 1976.
- M. Y. H. Bangash. *Impact and explosion, Analysis and design*. Blackwell Scientific Publications, 1993. ISBN 0-632-02501-8.
- J. M. Biggs. *Introduction to Structural Dynamics*. McGraw-Hill, 1964. ISBN 07-005255-7.
- A. K. Chopra. *Dynamics of structures - Theory and applications to earthquake engineering*. Prentice Hall International Series in Civil Engineering and Engineering Mechanics. Prentice Hall, New Jersey, 1995. ISBN 0-13-855214-2.
- A. Soleiman Fallah and L. A. Louca. Pressure-impulse diagrams for elastic-plastic-hardening and softening single-degree-of-freedom models subjected to blast loading. *Journal of Impact Engineering*, 34:823–842, 2007.
- S. M. Han, H. Benaroya, and T. Wei. Dynamics of transversely vibrating beams using four engineering theories. *Journal of Sound and Vibration*, 225(5):935–988, 1999.
- A. J. Kappos, editor. *Dynamic loading and design of structures*, chapter Loading from

- explosions and impact, pages 231–284. Spon Press, London, 2002.
- W. Karthaus and J. W. Leussink. Dynamic loading: more than just a dynamic load factor. *Proceedings of the First Symposium on the Interaction of nonnuclear munitions with structures*, 1983.
- T. Krauthammer, S. Astarlioglu, J. Blasko, T. B. Soh, and P. H. Ng. Pressure-impulse diagrams for the behavior assessment of structural components. *International Journal of Impact Engineering*, 35:771–783, 2008.
- Q. M. Li and H. Meng. Pressure-impulse diagram for blast loads based on dimensional analysis and single-degree-of-freedom model. *Journal of engineering mechanics*, 128(1): 87–92, 2002a.
- Q. M. Li and H. Meng. Pulse loading shape effects on pressure-impulse diagram of an elastic-plastic, single-degree-of-freedom structural model. *International journal of mechanical sciences*, 44:1985–1998, 2002b.
- G. W. Ma, H. J. Shi, and D. W. Shu. P-i diagram method for combined failure modes of rigid-plastic beams. *International Journal of Impact Engineering*, 34:1081–1094, 2007.
- Y. Shi, H. Hao, and Z.-X. Li. Numerical derivation of pressure-impulse diagrams for prediction of rc column damage to blast loads. *International Journal of Impact Engineering*, 35:1213–1227, 2008.
- P. D. Smith and J. G. Hetherington. *Blast and Ballistic Loading of Structures*. Elsevier Science. Butterworth-Heinemann, Oxford, 1994. ISBN 0-7506-2024-2.
- W. T. Thomson. *Theory of vibration with applications*. Prentice Hall, 1988. ISBN 0-04-445069-9.
- US Army, Navy and Air Force. Structures to resist the effect of accidental explosions. Technical report, Departments of the US Army, Navy and Air Force, 1990.
- L. J. Van der Meer. Dynamic response of high-rise building structures to blast loading. Master's thesis, Eindhoven University of Technology, 2008. Research report A-2008.3, O-2008.8.
- VROM. Publicatiereeks gevaarlijke stoffen 1, deel 2b: Effecten van explosie op constructies (in Dutch). Technical report, Ministerie van Binnenlandse Zaken en Koninkrijksrelaties, Ministerie van Verkeer en Waterstaat, 2003.

A List of symbols

All dimensionless parameters which have a dimensional equivalent are denoted with a bar. For example, the dimensional parameter a has a dimensionless equivalent \bar{a} .

A	area of beam cross section in m^2
a_c	critical wave number as in (8)
a_n	first wave number of mode n
α	γ^2/s^2
b_n	second wave number of mode n
β	a factor depending on pulse shape
C_n	constant which determines amplitude of mode shape
$c_{bs;n}$	modal contribution factor for base shear
$\bar{D}_n(\bar{t})$	time dependent dynamic load factor
$\bar{D}_{n;max}$	dynamic load factor
δ_{nm}	Kronecker delta which is 1 as $n = m$ and 0 otherwise
E	Young's modulus in N/m^2
ε	fraction of total response that is not accounted for
F_{eq}	equivalent load
\bar{F}_n	participation factor as in (14)
$\bar{F}(\bar{t})$	dimensionless pulse shape as in (12)
f	dimensionless load as in (38)
$\Psi_n(\bar{x})$	mode shape for rotation due to bending moment
$\varphi_n(\bar{x})$	rotation due to bending moment in mode n
G	Shear modulus in N/m^2
γ	material parameter as in (3)
H	height of beam in x -direction in m
I	second moment of area of beam cross section in m^4
i	dimensionless impulse as in (39)
j	imaginary unit
K_{eq}	equivalent stiffness
m	mass per unit length in kg/m
\bar{m}	$mH^4\omega_1^2/EI$
M_{eq}	equivalent mass
$\mu(x, t)$	moment in mode n
$\bar{\mu}(\bar{x}, \bar{t})$	$\mu(\bar{x}, \bar{t})H/EI$

$\bar{\mu}_b(\bar{t})$	base moment response of mode n
$\bar{\mu}_{b;c}$	critical base moment
$\bar{\mu}_{b;n}$	base moment in mode n
$\bar{\mu}_{b;st}$	static base moment: $\int_0^1 \bar{x}\bar{P}(\bar{x})d\bar{x}$
$\bar{M}_n(\bar{x})$	spatial distribution of internal moments in mode n
n	mode number
ω_1	fundamental natural frequency in rad
$\omega_{1;st}$	fundamental natural frequency by ESM using $\bar{y}_{st}(\bar{x})$
ω_n	natural frequency in rad
$\bar{\omega}_n$	ω_n/ω_1 .
$P(x)$	spatial load distribution in N/m
$\bar{P}(\bar{x})$	$P(\bar{x})H^3/EI$
P_m	uniform load distribution in N/m
\bar{P}_m	\bar{P}_mH^3/EI
r_c	critical response quantity
r_{dyn}	dynamic response
r_{st}	static response
s	geometry parameter: slenderness ratio as in (3)
t	time in s
\bar{t}	$\omega_1 t$
t_d	blast duration in s
\bar{t}_d	$\omega_1 t_d$
T_n	natural period of n^{th} mode
$u(t - t_0)$	unit step function which is 0 before t_0 and 1 after t_0
$\bar{V}_n(\bar{x})$	spatial distribution of internal shear forces
$\bar{v}_b(\bar{t})$	base shear response of mode n
$\bar{v}_{b;c}$	critical base shear
$\bar{v}_{b;ds}$	internal base shear in static deflected shape
$\bar{v}_{b;ms}$	internal base shear in first mode shape
$\bar{v}_{b;n}$	base shear in mode n
$\bar{v}_{b;st}$	static base shear: $\int_0^1 \bar{P}(\bar{x})d\bar{x}$
$v_n(x, t)$	shear in mode n
$\bar{v}_m(\bar{x}, \bar{t})$	$v_n(\bar{x}, \bar{t})H^2/EI$
$W_n(x)$	mode shape for transverse deflection including shear
$\bar{W}_n(\bar{x})$	$W_n(\bar{x})/H$

x	axial coordinate of beam as in Figure 2a
\bar{x}	x/H
$y(x)$	transverse deflection in m
$y_n(x, t)$	transverse deflection of mode n
$\bar{y}_1(\bar{x})$	dynamic deflected shape in first mode $\bar{F}_1 \bar{W}_1(\bar{x})$
$\bar{y}_n(\bar{x}, \bar{t})$	$y_n(x, t)/H$
$\bar{y}_{st}(\bar{x})$	static deflected shape